The chromatin-binding domain of Ki-67 together with p53 protects human chromosomes from mitotic damage

Osama Garwain[a], Xiaoming Sun[a,1], Divya Ramalingam Iyer[a,2], Rui Li[a], Lihua Julie Zhu[a], and Paul D. Kaufman[a,3]

[a]Department of Molecular, Cell and Cancer Biology, University of Massachusetts Medical School, Worcester, MA 01605

Edited by Bruce W. Stillman, Cold Spring Harbor Laboratory, Cold Spring Harbor, NY, and approved June 7, 2021 (received for review October 21, 2020)

Vertebrate mammals express a protein called Ki-67 which is most widely known as a clinically useful marker of highly proliferative cells. Previous studies of human cells indicated that acute depletion of Ki-67 can elicit a delay at the G1/S boundary of the cell cycle, dependent on induction of the checkpoint protein p21. Consistent with those observations, we show here that acute Ki-67 depletion causes hallmarks of DNA damage, and the damage occurs even in the absence of checkpoint signaling. This damage is not observed in cells traversing S phase but is instead robustly detected in mitotic cells. The C-terminal chromatin-binding domain of Ki-67 is necessary and sufficient to protect cells from this damage. We also observe synergistic effects when Ki-67 and p53 are simultaneously depleted, resulting in increased levels of chromosome bridges at anaphase, followed by the appearance of micronuclei. Therefore, these studies identify the C terminus of Ki-67 as an important module for genome stability.

DNA damage | mitosis | chromatin

Mammalian proliferation antigen Ki-67 has well-established clinical significance because of its utility as a marker for aggressive tumor cells (reviewed in ref. 1). Ki-67 is rapidly degraded during the G1 phase of the cell cycle, so quiescent or slowly growing cells that have long G1 phases generally have low levels of Ki-67 (2). In contrast, rapidly growing cells, including tumor cells that lack checkpoint controls, often have short G1 phases and thereby display high steady-state Ki-67 levels (3). High Ki-67 protein levels are correlated with the severity of many types of tumors, and are strongly predictive of poor outcomes in meta-analyses of clinical cancer data (4–7). Recent experiments also show that Ki-67 is important for tumor growth and metastasis (8). As we describe below, Ki-67 is critical for maintaining several aspects of chromosome structural integrity. Therefore, molecular exploration of these functions is crucial to understanding how Ki-67 contributes to tumor biology.

Clues regarding the multiple functions of Ki-67 come from its dramatic relocalization across the cell cycle (1, 9, 10). In interphase cells, Ki-67 is localized to the nucleolus and is required for efficient localization of heterochromatin to the nucleolar periphery (11–13). Depletion of Ki-67 also alters the focal accumulation of the heterochromatic histone modification H3K9me3 (12) and the modification and localization of nucleolus-associated inactive X chromosomes (14). After interphase, Ki-67 localization dramatically changes when it becomes heavily phosphorylated by CDK1 during mitotic entry (15, 16). Ki-67 coats mitotic chromosomes, serving as a fundamental component of the perichromosomal layer [PCL (11, 17); reviewed in refs. 1, 18, and 19]. The PCL is the mitotic repository of the abundant ribonucleoprotein complexes that inhabit the nucleolus during interphase (19, 20). Without Ki-67, the PCL is absent, dispersing these components (11, 17), causing imbalanced inheritance of nucleolar material in daughter cells (11). During mitosis, Ki-67 has additional key functions: It is required for maintenance of spatially separated chromosome arms (21, 22) and also for the clustering of chromosomes prior to nuclear envelope reformation, thereby preventing retention of cytoplasmic material when nuclei reassemble after mitosis (23). Tethered to chromatin, the long and highly charged Ki-67 protein serves as an electrostatic repellant that prevents chromosome arms from clumping (21, 22). This pathway is distinct from the contribution of condensin proteins to mitotic chromosome structure, because codepletion of both Ki-67 and condensin results in synergistic loss of nearly all mitotic chromosome structure (24). In sum, Ki-67 shapes chromosome architecture in both interphase and mitotic cells.

In our previous studies, we had observed that acute depletion of Ki-67 causes a delay in cell-cycle progression at the G1/S transition of the cell cycle in checkpoint-proficient cells (14). This delay is accompanied by induction of the cyclin-dependent kinase inhibitor p21, which is required for the delay (14). p21 is a transcriptional target of the tumor suppressor protein p53 (25, 26), a critical activator of the transcriptional response to DNA damage. These observations led us to test whether Ki-67 protects cells from DNA damage, and whether p53 has a role. We show here that acute depletion of Ki-67 results in DNA damage as evidenced by increased levels of modified histone γH2AX, focal accumulation of repair signaling protein 53BP1, and detection of

Significance

Ki-67 is a clinically important tumor proliferation marker protein. Ki-67 contributes to the three-dimensional organization of heterochromatin during interphase of the cell cycle, and also coats and shapes condensed chromosomes during mitosis. Here, we show that acute depletion of Ki-67 in human cells causes DNA damage as cells traverse mitosis. When the tumor suppressor protein p53 is codepleted with Ki-67, multiple hallmarks of genome instability arise, including anaphase chromosome bridges, followed by the appearance of micronuclei. The C-terminal chromatin-binding domain of Ki-67 is sufficient for resistance to this damage. These studies uncover a factor for genome maintenance and identify a protective protein domain.

Author contributions: O.G., X.S., D.R.I., and P.D.K. designed research; O.G., X.S., D.R.I., and P.D.K. performed research; O.G., R.L., L.J.Z., and P.D.K. analyzed data; and O.G. and P.D.K. wrote the paper.

The authors declare no competing interest.

This article is a PNAS Direct Submission.

[1]Present address: School of Statistics, Xi'an University of Finance and Economics, Xi'an 710100, People's Republic of China.

[2]Present address: Department of Radiation Oncology, Dana-Farber Cancer Institute and Harvard Medical School, Boston, MA 02215.

[3]To whom correspondence may be addressed. Email: paul.kaufman1@umassmed.edu.

This article contains supporting information online at https://www.pnas.org/lookup/suppl/doi:10.1073/pnas.2021998118/-/DCSupplemental.

Published August 5, 2021.

broken DNA strands via terminal transferase labeling. This damage accumulates during mitotic progression both in cells that display a checkpoint response to Ki-67 depletion and in cells that do not, indicating that the role of Ki-67 in genome stability is independent of a transcriptional response to damage. We demonstrate that the C-terminal chromatin-binding domain of Ki-67 is necessary and sufficient to protect cells from this damage. These data define a genome protection molecule, and indicate that this activity is distinct from Ki-67's role in maintaining distinct chromosome arm structures, which requires additional parts of the protein to provide sufficient electrostatic repulsion (22). We also show that loss of Ki-67 causes greater defects in the absence of tumor suppressor protein p53, including a large increase in the numbers of anaphase bridges that appear during the first mitosis after acute Ki-67 depletion. Subsequently, cells lacking Ki-67 and p53 frequently display micronuclei that lose lamin A protein from their periphery over time, a hallmark of membrane disruption associated with genome rearrangements (27, 28). In sum, these data indicate that Ki-67 physically protects chromosomes from damage during mitosis.

Results

Ki-67 Protects Cells from DNA Damage Regardless of G1/S Checkpoint Status. To test whether acute depletion of Ki-67 causes DNA damage, we first analyzed cells by immunofluorescence (IF) using antibodies that recognize γH2AX, a phosphorylated histone isoform that is a classical marker of DNA strand breaks (29). We initially analyzed hTERT-RPE1 cells, a diploid, checkpoint-proficient human cell line, which display a p21-dependent transcriptional program in response to Ki-67 depletion (14). Using the same small interfering RNA (siRNA) duplex we had validated previously in RPE1 cells (14), we tested acute depletion of Ki-67 in an asynchronous cell population, thereby sampling all cell-cycle positions. We observed that depletion of Ki-67 significantly increased the γH2AX signals (Fig. 1*A*), and that the magnitude of this effect was amplified in the presence of the DNA strand–breaking reagent phleomycin [Fig. 1*B* (30)]. These data suggested that DNA damage occurs upon acute depletion of Ki-67.

Our previous studies showed that upon acute depletion of Ki-67, RPE1 cells display a transient cell-cycle delay at the G1/S boundary, accompanied by p21-dependent down-regulation of many S phase–related transcripts (14). Therefore, we considered the possibility that the transcriptional response to Ki-67 depletion was indirectly causing DNA damage. To test this idea, we analyzed a cell line that lacks this transcriptional response, colon cancer HCT116 cells. Specifically, we used a derivative of this well-studied line in which homozygous in-frame insertions encode Ki-67 tagged with a fluorescent mClover protein and an auxin-inducible degron (21), which allows rapid depletion of detectable Ki-67 upon addition of auxin (indole acetic acid; IAA). We confirmed that these HCT116-Ki-67-mAC cells (henceforth HCT116 for brevity), unlike RPE1 cells but similar to virally transformed HeLa cells, do not induce p21 messenger RNA (mRNA) levels in response to Ki-67 depletion (*SI Appendix*, Fig. S1*A*). Furthermore, RNA-sequencing (RNA-seq) analysis of HCT116 cells detected an extremely limited genome-wide transcriptional response to acute Ki-67 depletion (*SI Appendix*, Fig. S1 *B–D* and Dataset S1). Nevertheless, after 24 h of auxin-mediated depletion of Ki-67, γH2AX signals were significantly increased in these cells (Fig. 1 *C* and *D*). Together, these data indicate that Ki-67 has a role in genome stability in multiple cell types.

These data also suggested that the contribution of Ki-67 to genomic stability is independent of the p21-mediated transcriptional response. To test this directly, we codepleted p21 and Ki-67. We observed that depletion of p21 did not significantly change the levels of γH2AX generated either in the absence or presence of Ki-67, even when the assay was sensitized by the presence of phleomycin (*SI Appendix*, Fig. S2 *A–C*). These data are consistent with our finding that the damage caused by depletion of Ki-67 does not depend on checkpoint signaling (Fig. 1). We therefore hypothesized that Ki-67 has a direct role in protecting the genome from damage.

53BP1 Foci and DNA Strand Breaks Are Formed upon Depletion of Ki-67. Our discovery of DNA damage upon Ki-67 depletion was surprising because a previous study discounted the possibility of a contribution to DNA protection by Ki-67, because no 53BP1 foci were detected in cells lacking Ki-67 (11). 53BP1 forms large foci at sites of DNA damage and is instrumental in regulating the choices between homologous recombination and end-joining repair pathways (31–34). Because of our observation of robust γH2AX signals, we reexamined whether Ki-67 depletion results in 53BP1 focus formation. Indeed, we find that it does (Fig. 1 *D* and *E*), consistent with Ki-67 having an important role in genome protection. These 53BP1 foci were frequently overlapping γH2AX foci, consistent with the documented direct recruitment of 53BP1 by γH2AX (35). 53BP1 was not detected in mitotic cells regardless of the amount of DNA damage (*SI Appendix*, Fig. S2*D*), consistent with previous experiments demonstrating that 53BP1 foci are not present in mitotic cells (36, 37).

In addition to γH2AX and 53BP1 protein foci, we tested whether we could directly detect broken DNA strands upon acute depletion of Ki-67. To do this, we performed terminal deoxynucleotidyl transferase dUTP nick end labeling (TUNEL) assays, in which broken DNA strands are detected as substrates for template-independent extension by the enzyme terminal deoxynucleotide transferase [TdT (38, 39)]. We analyzed HCT116 cells, using fluorescence-activated cell sorting (FACS) to simultaneously monitor mClover-tagged Ki-67 and also TdT-mediated incorporation of the modified deoxynucleotide 5-ethynyl-2-deoxyuridine (EdU), labeled via click-chemistry addition of a fluorescent (595-nm) azide. We observed that untreated cells displayed very little azide signal (Fig. 1 *G* and *H*). In contrast, IAA-mediated depletion of Ki-67 resulted in robust TUNEL labeling (Fig. 1 *I* and *J*). We conclude that acute depletion of Ki-67 causes DNA strand breaks.

Ki-67 Protects Chromosomes during Mitosis. In Fig. 1, asynchronous populations were analyzed, so that cells across all points of the cell cycle had experienced the absence of Ki-67. We next sought to determine whether the role of Ki-67 in protection of chromosomes from damage might be important at specific times during the cell cycle. We first tested whether damage occurred during S phase. To do this, we pulse-labeled asynchronous HCT116 cell cultures with EdU for 20 min prior to fixation, followed by click-chemistry staining to detect cells that synthesized DNA during the pulse. The control population that was untreated with auxin did not display strong γH2AX signals, neither in the EdU-positive subpopulation that had been in S phase, nor in the mitotic subpopulation that displayed chromosome condensation (Fig. 2 *A–C*). In the IAA-treated population, we observed that the S phase subpopulation also lacked strong γH2AX signals. In contrast, the mitotic auxin-treated cells displayed robust γH2AX staining. These data suggested that mitosis is a particularly important time for genome protection by Ki-67.

To test this more directly, we synchronized HCT116 cells at the G2/M phase border with the CDK1 inhibitor RO-3306 (40), depleted Ki-67 using auxin, and then measured damage before and after release. We analyzed γH2AX levels via IF (Fig. 2*D*) and FACS measurements (*SI Appendix*, Fig. S3*A*); we also detected strand breaks via TUNEL assays (*SI Appendix*, Fig. S3*B*). In these assays, unreleased cells in the presence of RO-3306 displayed low levels of damage (*SI Appendix*, Fig. S3). However, in cells depleted of Ki-67, but not in control untreated cells,

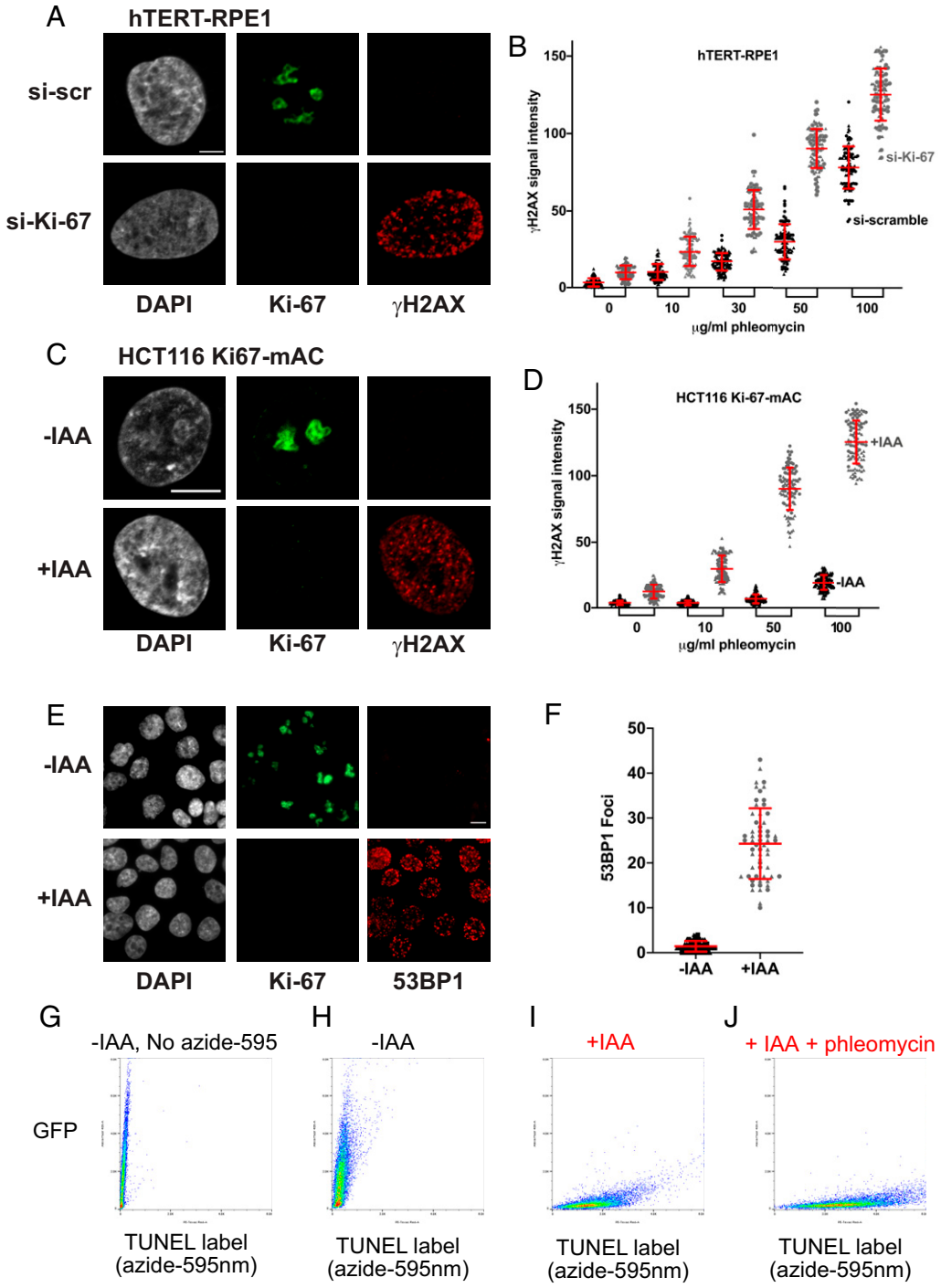

Fig. 1. γH2AX, 53BP1, and TUNEL staining in Ki-67–depleted cells. (*A*) hTERT-RPE1 cells were treated with si-scr or si-Ki-67 as indicated for 72 h. DNA was stained with DAPI (gray), and Ki-67 (green) and γH2AX (red) were detected by immunofluorescence. (*B*) hTERT-RPE1 cells were treated as in *A*, in the presence or absence of the indicated amounts of phleomycin. γH2AX signals from 50 cells of each population are graphed for two independent biological replicate experiments (distinguished by circles versus triangles). si-scramble–treated cells are depicted in black; si-Ki-67–treated cells are in gray. Mean values and SDs among all cells for each condition are indicated in red. Ki-67 depletion significantly increased γH2AX signals for all doses of phleomycin ($P < 0.0001$, Welch's *t* test). (*C*) HCT116-Ki-67-mAC cells (HCT116 cells) were either untreated (–IAA) or treated with indole acetic acid (+IAA) for 24 h to deplete Ki-67 and analyzed as in *A*, except that Ki-67 was detected via fluorescence of the mClover tag. (*D*) Quantitation of γH2AX in HCT116 cells, as in *B*. Ki-67 depletion significantly increased γH2AX signals at all doses of phleomycin ($P < 0.0001$, Welch's *t* test). (*E*) HCT116 cells were treated as indicated and prepared for IF with antibodies recognizing 53BP1 (red). Green-channel fluorescence detected mClover-tagged Ki-67. (*F*) 53BP1 foci were counted in 30 cells in each population from two biological replicate experiments as in *E* and graphed as in *B* and *D*. Ki-67 depletion significantly increased numbers of 53BP1 foci ($P < 0.0001$, Welch's *t* test). (*G–J*) TUNEL labeling detects DNA strand breaks in Ki-67–depleted cells. HCT116 cells were analyzed by two-dimensional FACS to detect the GFP-labeled Ki-67 protein (*y* axis) or EdU coupled to fluorescent azide-595 nm to measure strand breaks (*x* axis). (*G*) HCT116 cells were treated with terminal transferase + EdU to label strand breaks, but without the azide-594 nm fluorescent label, thereby indicating the background signal level. (*H*) Untreated HCT116 cells display very low damage signals. (*I*) HCT116 cells were treated with auxin (IAA) to trigger degradation of Ki-67. The GFP label on Ki-67 is lost, and DNA damage appears. (*J*) Cells were treated with IAA plus 30 μg/mL phleomycin, resulting in an even greater DNA damage signal, indicating the assay is not saturated. (Scale bars, 5 μm.)

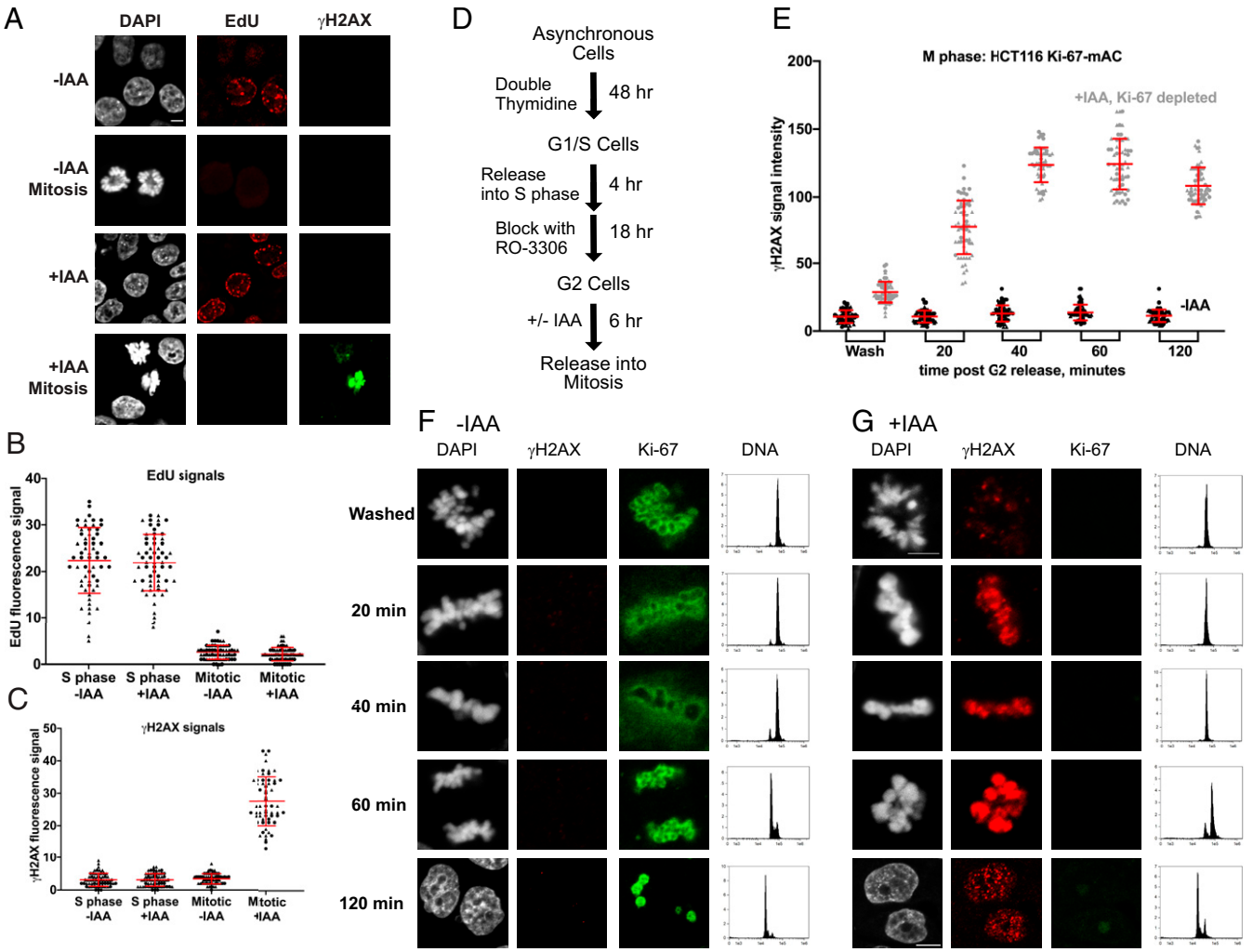

Fig. 2. Ki-67 depletion causes damage during mitotic progression. (*A*) HCT116 cells were treated or untreated with IAA for 5 h as indicated, and pulse-labeled with EdU (red) 30 min prior to fixation for IF detection of γH2AX (green). Mitotic cells in these asynchronous populations are indicated separately. (Scale bar, 5 μm.) (*B*) EdU signals in 30 cells of each of the indicated populations were quantified. "S phase" cells displayed visible EdU signals; "mitotic" cells were those that displayed condensed chromosomes. (*C*) The γH2AX signals in the same cells analyzed in *B* are displayed. (*D*) Scheme for cell synchronization. (*E*) γH2AX signal intensity was measured in 30 cells in each of the control (–IAA) and auxin-treated (+IAA) populations from the indicated time points after release from RO-3306 arrest. (*F* and *G*) IF analysis of individual cells from the indicated time points in (*F*) –IAA and (*G*) +IAA experiments. DAPI (gray), γH2AX (red), and Ki-67–mClover (green) are shown. (*F* and *G*, *Right*) Amnis FACS analysis of the DNA content of DAPI-stained cells treated in the same manner as cells analyzed by IF. (Scale bars, 5 μm.) The fields displaying cells from the 120-min time point are slightly larger to capture two cells.

γH2AX and TUNEL labeling levels increased immediately after washout of RO-3306 (Fig. 2 *E*–*G* and *SI Appendix*, Fig. S3). These data suggested that Ki-67 has a particularly important role in genome protection as cells prepare for mitosis. Furthermore, the rapid appearance of damage in these synchronized cell experiments suggests that this damage is unlikely to result from indirect transcriptional effects, consistent with the limited transcriptional effects of Ki-67 depletion in HCT116 cells (*SI Appendix*, Fig. S1).

DNA damage could occur if Ki-67 depletion triggered the activity of caspase-dependent deoxyribonucleases (41). To test this, we analyzed synchronized cells as before, comparing γH2AX signals in the absence or presence of pan-caspase inhibitor zVAD-FMK (42) (*SI Appendix*, Fig. S4*A*). We observed that zVAD-FMK treatment did not affect the appearance of γH2AX. As a positive control for the effectiveness of this inhibitor, we showed that it would reduce the DNA fragmentation caused by the apoptosis-inducing drug camptothecin (43, 44) (*SI Appendix*, Fig. S4*B*). Together, these data suggested that the strand breaks appearing in the absence of Ki-67 were not caused by caspase-dependent nuclease activity. Instead, these experiments supported the idea that Ki-67 has a direct role in protecting chromosomes.

The C-Terminal Chromatin-Binding Domain of Ki-67 Is Necessary and Sufficient for Protecting Chromosomes. To determine whether specific domains of Ki-67 protect chromosomes from damage, we used HCT116 cells to establish an assay for Ki-67 transgenes. We transiently transfected plasmids encoding various green fluorescent protein (GFP)–tagged Ki-67 fragments (16) into asynchronous cell populations. Twelve hours later, we added auxin (IAA) and continued incubation for 24 h to degrade endogenous Ki-67 and allow accumulation of damage, and then measured γH2AX and GFP signals by FACS and IF analyses. We first confirmed that in untransfected cells, low levels of γH2AX staining (right-hand side of the graph, percentage indicated

above) were detected in more than 90% of the cells in the absence of auxin treatment (−IAA; Fig. 3*A*). Conversely, high levels of damage were observed upon auxin treatment, with fewer than 10% of cells displaying γH2AX levels similar to the untreated population (+IAA; Fig. 3*A*). We also noted that GFP signals were greatly decreased by auxin treatment, indicating efficient degron-mediated destruction of the endogenous mClover-tagged Ki-67 protein. We then analyzed transfected cells treated with IAA. In empty vector (enhanced GFP; EGFP)–transfected cells, most cells displayed high GFP levels, but few undamaged cells were observed (Fig. 3*B*). In contrast, transfection of a wild-type Ki-67 transgene also increased GFP levels but prevented most cells from displaying high levels of damage (Fig. 3*B*). Therefore, this assay was able to detect chromosome protection by Ki-67 transgenes. We then tested a series of deletion constructs (Fig. 3*C*), and observed that all constructs encoding the C-terminal chromatin-binding domain protected cells from elevated γH2AX levels, and all constructs that lack this domain did not (Fig. 3 *D* and *E*). We confirmed that Ki-67 derivatives containing the C-terminal chromatin-binding domain robustly localized to the chromosomes during the critical mitotic period, and those that lack this domain did not (*SI Appendix*, Fig. S5). We conclude that the C terminus of Ki-67, which is the chromosome-binding domain (16, 22, 45), is necessary and sufficient for genome protection.

Synergies upon Codepletion of p53. In contrast to the effects of p21 depletion (14) (*SI Appendix*, Fig. S2), we observed a dramatic loss of viability in hTERT-RPE1 cells when Ki-67 and p53 were depleted simultaneously (Fig. 4 *A* and *B*). We also observed synergy with p53 depletion in HCT116 cells, although in this case reduced proliferation rather than lethality was observed (Fig. 4*C*). As before, when p53 was present (Fig. 2 and *SI Appendix*, Fig. S3), codepletion of Ki-67 and p53 caused robust γH2AX and TUNEL labeling after release into mitosis (Fig. 4 *D–F* and *SI Appendix*, Fig. S6 *A* and *B*). We demonstrated that the increased levels of γH2AX observed upon depletion of both Ki-67 and p53 were blocked by cotransfection of plasmids encoding either Ki-67 or an siRNA-resistant p53 complementary DNA (cDNA), but not the empty vector (*SI Appendix*, Fig. S6*C*). Furthermore, we demonstrated that the level of γH2AX induced upon mitotic entry when both Ki-67 and p53 were depleted was not affected by treatment with zVAD-FMK (*SI Appendix*, Fig. S7*A*).

To determine whether the same domain of Ki-67 protects cells in the absence of p53, we repeated the previous transgene complementation assay in HCT116 cells treated with si-p53. Again, the C-terminal leucine-arginine–rich (LR) domain was necessary and sufficient for protection, with the magnitude of the γH2AX signals greater in the absence of p53 (*SI Appendix*, Fig. S7 *B–E*). We also confirmed the synergistic damage phenotypes using a second siRNA that targets p53 (*SI Appendix*, Fig. S8 *A–D*). Further, we demonstrated that the synthetic lethality caused by codepletion of Ki-67 and p53 in hTERT-RPE1 cells was prevented by cotransfection of a plasmid expressing the LR domain of Ki-67, or expressing a p53 cDNA that lacks the siRNA target in the natural 3′ untranslated region of the *TP53* gene encoding p53. In contrast, an empty pEGFP vector plasmid did not prevent lethality (*SI Appendix*, Fig. S9*A*). Together, these data confirmed the on-target effects of siRNA-mediated p53 depletion, and indicated that the genomic damage caused by the lack of the Ki-67 C-terminal domain is magnified in the absence of p53.

The damage caused by codepletion of Ki-67 and p53 was also qualitatively different: We observed more frequent structures resembling anaphase bridges (DNA stretched between both segregating chromosome masses) (Fig. 5 *A* and *B*). Anaphase bridges arise from telomeric fusions or from misrepair of DNA damage, and are increased upon exposure to a wide variety of genotoxic agents (46). Observation of anaphase bridges is significant because they contribute to aneuploidy, a very frequent feature of human tumors (47). We observed other anaphase defects with a variety of appearances, in some cases including separated DNA masses resembling lagging chromosomes (*SI Appendix*, Fig. S8*E*). We quantified the appearance of anaphase defects in RO-3306–synchronized mitoses in HCT116 cells, either with or without IAA-driven Ki-67 degradation, and either with or without p53 depletion. We observed that anaphase defects were by far most abundant in doubly depleted cells (Fig. 5*A*), and that they began to appear 60 min post release, around the time of sister chromosome separation at anaphase (Figs. 4 *E*, *F*, and 5*B*). These observations suggested that significant genome instability is triggered upon codepletion of Ki-67 and p53.

Indeed, in addition to anaphase defects, microscopic examination indicated additional abnormal nuclear morphologies upon codepletion of Ki-67 and p53. After the synchronized cells passed through mitosis in the absence of both Ki-67 and p53, these included grossly altered nuclear morphologies and strongly DAPI-stained puncta (Fig. 4*F*, 120-min time point). The doubly depleted cells also displayed small DAPI-stained bodies that appeared to be micronuclei (Fig. 5 *C–J*).

Previous studies have shown that anaphase DNA bridges can lead to formation of micronuclei (48, 49), which are small bodies containing single chromosomes or chromosome fragments enclosed within nuclear envelope–derived membranes (48). To confirm that these are micronuclei, we showed that these stained with antibodies recognizing LAP2a (Fig. 5 *D*, *E*, and *H–J*), a protein constitutively found in micronuclei (28). We also observed that after 24 h of auxin treatment, the micronuclei contained lamin A/C protein around their membrane but that after 48 h these levels were greatly reduced (Fig. 5 *F* and *G*). Such loss of lamin is characteristic of micronuclear envelope degradation (27, 28), a process by which DNA in micronuclei loses nuclear membrane integrity and becomes exposed to inappropriate action of DNA recombination and replication enzymes leading to genome rearrangements. These data reinforce the importance of Ki-67 in genome stability, and suggest that anaphase bridges formed during the first mitosis after Ki-67 loss later become micronuclei. Similar genomic instability cascades are well-documented in the formation of aneuploid cells (50). We note that the appearance of micronuclei in cells depleted of both Ki-67 and p53 was prevented by transfection of plasmids encoding either full-length Ki-67 or the LR domain, but not by an empty vector (*SI Appendix*, Fig. S9*B*). The LR domain was also sufficient to prevent elevated levels of anaphase defects during mitosis in the absence of Ki-67 and p53 (*SI Appendix*, Fig. S9*C*), and also to prevent accumulation of large numbers of 53BP1 foci in the following G1 phase (*SI Appendix*, Fig. S9*D*). Therefore, the LR domain was sufficient for Ki-67's contribution to genome stability throughout these studies.

Recent studies have indicated that defects in DNA replication or broken chromosome bridges formed during interphase can result in aberrant DNA synthesis during subsequent mitoses, on a path toward high levels of genome instability (51, 52). We did not detect DNA synthesis in Ki-67–depleted mitotic cells (Fig. 2 *A–C*). However, given our findings regarding p53 (Fig. 4), we also tested for DNA synthesis in mitotic cells after acute codepletion of Ki-67 and p53. We labeled cells with EdU to detect DNA synthesis and also stained for LAP2a to enhance detection of micronuclei (Fig. 5 *H–J*). We observed frequent EdU labeling of interphase cells in this asynchronous population, with a similar percentage of EdU-positive micronuclei. In contrast, no EdU-positive mitotic cells were detected (Fig. 5*I*). These data suggest that unscheduled DNA synthesis during mitosis is not a prominent outcome of Ki-67 depletion, either with or without codepletion of p53. These data also reinforce our conclusion that mitosis is the critical period for genome protection by Ki-67.

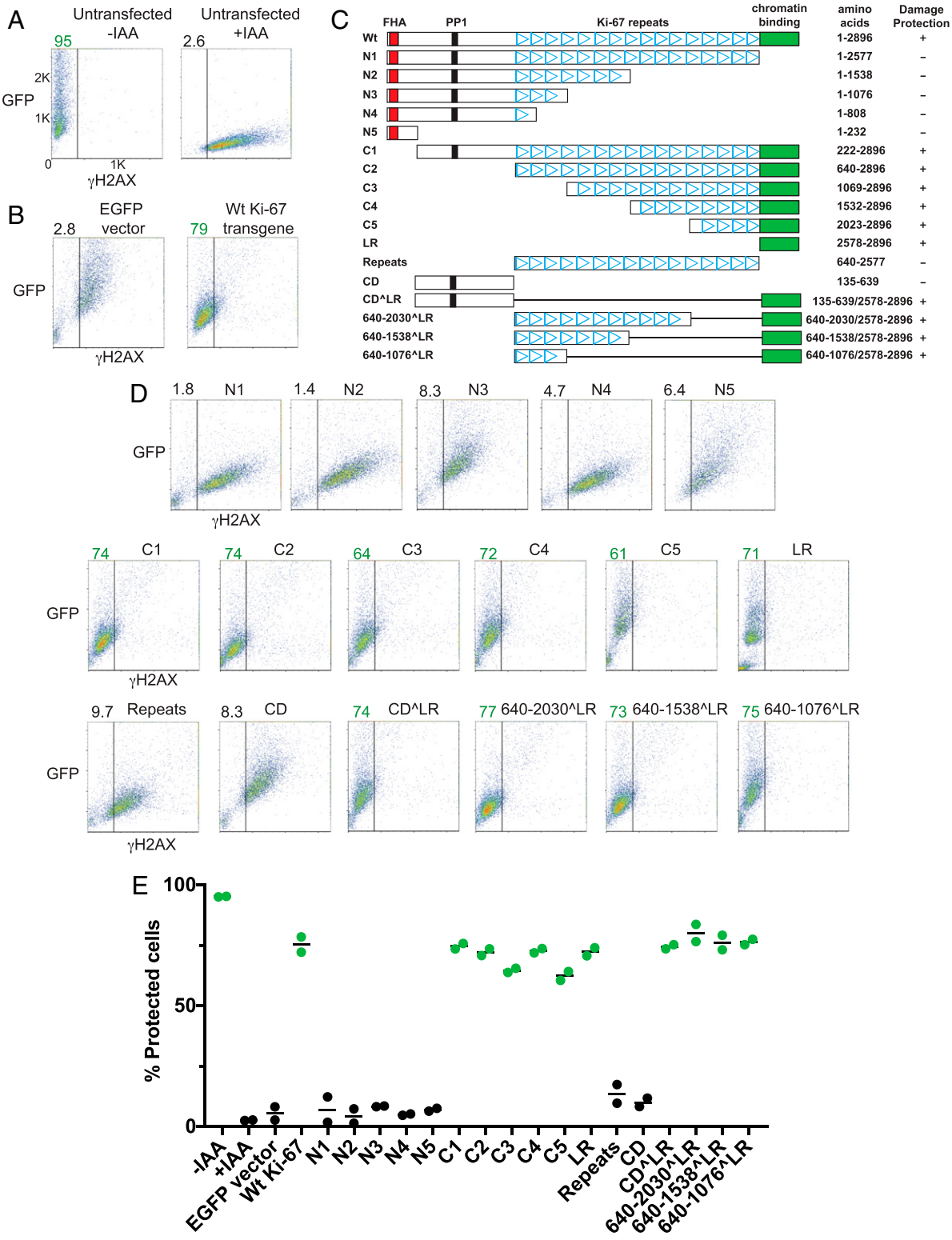

Fig. 3. C-terminal domain of Ki-67 protects cells from damage. (*A*) Two-dimensional (2D) FACS analysis of HCT116 cells, with GFP-channel intensity on the *y* axis and γH2AX signal intensity on the *x* axis. Untransfected cells were either untreated (–IAA) or treated with auxin (+IAA). IAA treatment resulted in degradation of Ki-67–mClover, causing the loss of cells with low γH2AX signal intensity as well as fluorescence in the GFP channel. The percentages of cells with low γH2AX signal intensity (to the left of the vertical black line) are shown at the upper left corner. (*B*) Control experiments. Cells were transfected with the indicated constructs, treated with IAA, and analyzed by 2D FACS as above. Transfection of the empty vector (pEGFP-C1) restored GFP fluorescence to the majority of cells, but most cells displayed elevated γH2AX signal intensity. In contrast, transfection of a plasmid encoding GFP fused to a full-length Ki-67 cDNA resulted in most cells having reduced γH2AX signal intensity. (*C*) Schematic of transfected constructs. The FHA domain, protein phosphatase 1–binding domain, internal repeats (triangles), and C-terminal chromatin-binding LR domain (green) are indicated. (*D*) Two-dimensional FACS analysis of cells transfected with the indicated constructs. Constructs that resulted in the majority of cells displaying low γH2AX signal intensity ("protected") are tabulated in *C*. (*E*) Summary of data from biological replicate experiments. Treatments yielding a majority of "protected" cells are colored in green.

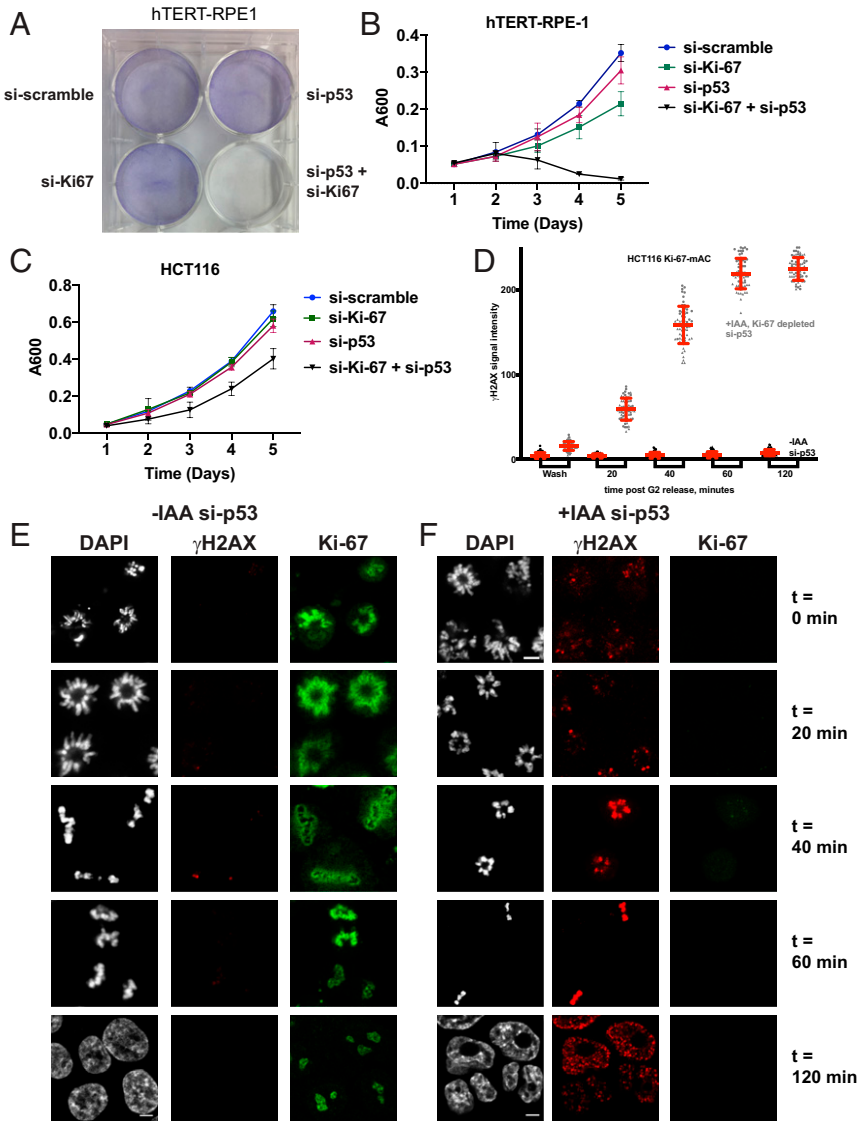

Fig. 4. Synergistic effects of codepletion of Ki-67 and p53. Experiments in this figure were performed using si-p53 (s606); companion experiments using the alternative si-p53 (s607) are shown in *SI Appendix*, Fig. S8. (*A*) Crystal violet staining of hTERT-RPE1 cells treated with the indicated siRNAs. (*B*) Proliferation of hTERT-RPE1 cells treated with the indicated siRNAs measured with Alamar blue. Data from eight replicate populations are shown. (*C*) Proliferation of HCT116 cells treated with the indicated siRNAs, measured as in *B*. (*D*) As in Fig. 3*B*, γH2AX was analyzed in RO-3306–synchronized HCT116 cells, except here cells were also treated with si-p53. (*E* and *F*) IF images of cells treated as in *D*. As in Fig. 3 *C* and *D*, the fields of the 120-min images are of slightly different size from the others. (Scale bars, 5 μm.)

Distinct Effects of Acute p53 Depletion versus a Preexisting Gene Deletion. Several recent studies have shown that the presence of p53 can dramatically alter the outcome of synthetic lethality screens (53–55). These and other studies have provided lists of genes that are synthetically lethal with p53, and we note that the *MKI67* gene encoding Ki-67 has not been found among these. We therefore wondered whether loss of Ki-67 in cells that already lack p53 would cause similarly severe phenotypes. To test this idea, we depleted Ki-67 in a derivative of hTERT-RPE1 cells in which both *TP53* alleles encoding p53 were deleted via CRISPR (56). As expected, treatment of these cells with si-p53 had no effect. Notably, the p53-null version of RPE1 cells was not killed by depletion of Ki-67 (*SI Appendix*, Fig. S10 *A* and *B*). Furthermore, unlike the wild-type RPE1 cells, these $p53^{-/-}$ cells did not display increased levels of DNA damage upon depletion of Ki-67, as measured via either IF or FACS analyses (*SI Appendix*, Fig. S10*C*). Therefore, the genetic environment can strongly affect the results of Ki-67 depletion. We hypothesize that during the serial passaging of the $p53^{-/-}$ cells in the course of selection and screening, there has been adaptation that overrides the genome instability that would otherwise be caused by loss of Ki-67.

Discussion

Acute Depletion of Ki-67 Causes DNA Damage That Originates during Mitosis. The role of Ki-67 in genome protection was most evident in mitotic cells, and was detected in the first mitosis after rapid depletion of the protein in the preceding G2 phase (Fig. 2). These data suggest that the damage observed in interphase cells originated during mitosis, and that the triggering events are not left over from unrepaired breaks or errors in a previous S phase. Rather, the rapid appearance of damage during progression through mitosis after acute depletion of Ki-67 leads us to favor the idea that Ki-67 directly protects mitotic chromosomes. In this view, the appearance of γH2AX is one more aspect of defective

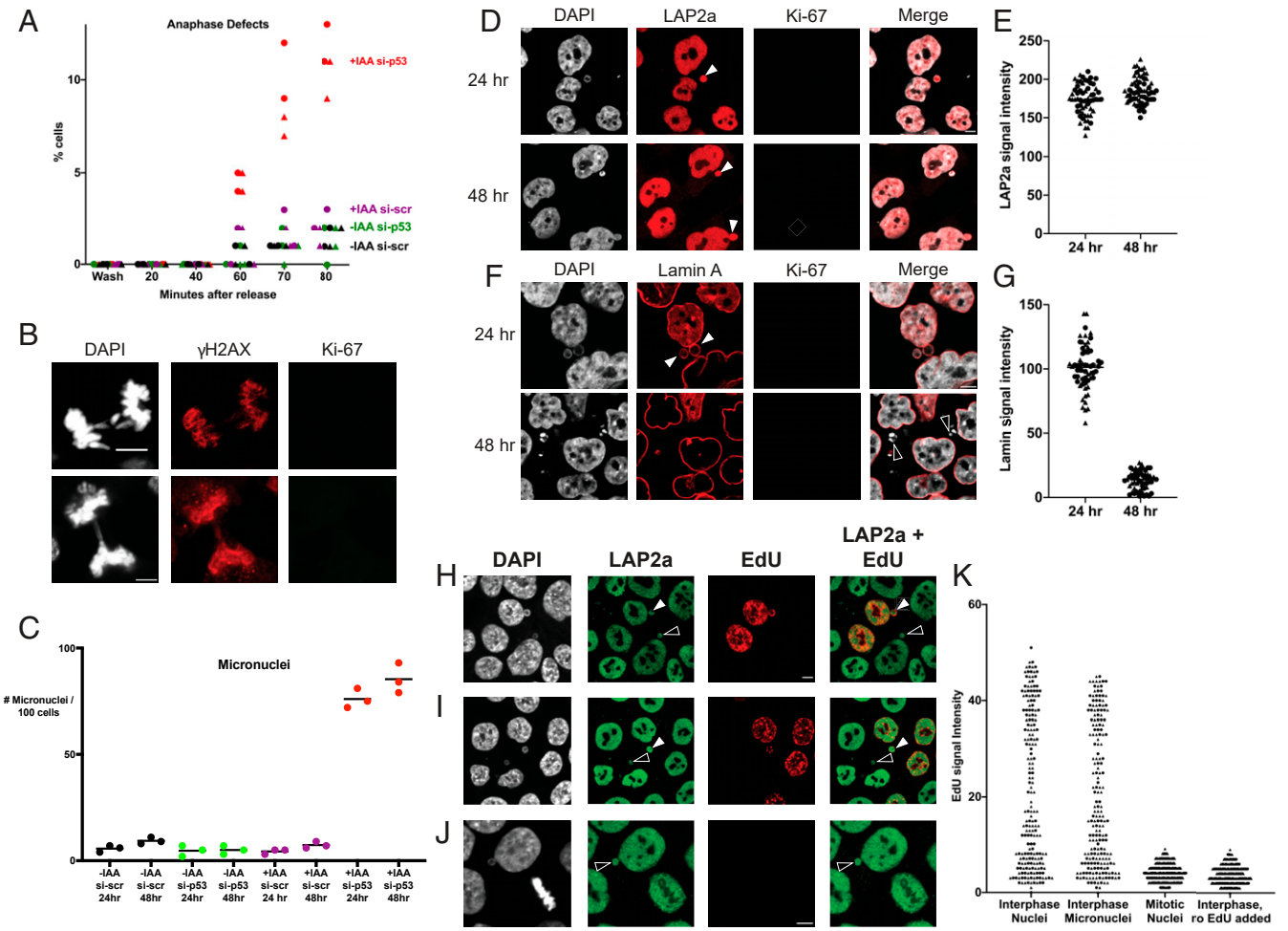

Fig. 5. Codepletion of Ki-67 and p53 increases the frequency of anaphase defects and micronuclei. (*A*) Quantitation of defects (bridges and lagging chromosomes) in RO-3306–synchronized HCT116 cells after the indicated treatments. Note that cells entering anaphase were first observed at the 60-min time point (Fig. 4 *E* and *F*). (*B*) Examples of anaphase defects from RO-3306–synchronized HCT116 cells treated with IAA + si-p53, from the 60-min point. Additional images are shown in *SI Appendix*, Fig. S8*E*. (*C*) Quantitation of micronuclei in HCT116 cells 24 or 48 h after the indicated treatments. (*D*) IF analysis of Lap2a in si-p53–treated cells for the indicated times after IAA treatment. Solid arrowheads indicate micronuclei with intact lamin A staining. (*E*) Quantitation comparing Lap2a staining from *D*. (*F*) As in *D*, IF analysis of lamin A in +IAA si-p53 cells. Solid arrowheads indicate micronuclei with intact lamin A staining. Open arrowheads indicate DAPI-stained bodies that lack lamin A staining, indicating micronuclei with degraded envelopes. (*G*) Quantitation of lamin A staining from *F*. (*H–J*) HCT116 cells were treated with si-p53 for 72 h and IAA for the final 24 h and then labeled with EdU for 20 min prior to fixation. (*K*) Quantitation of the EdU intensities of cells illustrated in *H–J*. Interphase cells, micronuclei observed in interphase cells, and mitotic cells were quantified as separate classes. Interphase cells that did not incorporate EdU were quantified as a negative control for background fluorescent signals. Solid arrowheads indicate micronuclei that incorporated EdU; open arrowheads indicate micronuclei that were not labeled. Field sizes are the same within panels and for *H* and *I*. (Scale bars, 5 μm.)

chromatin maintenance upon Ki-67 depletion, consistent with previously described structural deformations of heterochromatin (12), loss of association and modification of heterochromatin at the nucleolar periphery (11–14), and reduced transcriptional silencing of pericentromeric alpha-satellite repeats (57).

We observed γH2AX and 53BP1 foci in interphase cells upon acute depletion of Ki-67 (Fig. 1). These data suggest that DNA damage explains why checkpoint-proficient hTERT-RPE1 cells acutely depleted of Ki-67 trigger p21-dependent cell-cycle delays and transcriptional responses (14). We note that damage was observed both in hTERT-RPE1 cells that induce p21 in response to Ki-67 depletion and in HCT116 cells that do not display this response (Fig. 1). Therefore, the observed DNA damage is not dependent on the checkpoint-mediated transcriptional signature observed in Ki-67–depleted hTERT-RPE1 cells (14). Consistent with this conclusion, we observed that HCT116 cells display significantly altered levels of very few mRNAs upon Ki-67 depletion (*SI Appendix*, Fig. S1).

The C Terminus of Ki-67 Protects Chromosomes from Damage. Ki-67 is a very large protein (over 3,000 amino acids), and previous studies have characterized several functional subdomains (Fig. 3*C*; reviewed in ref. 1). At the N terminus is a phosphopeptide-binding forkhead-associated (FHA) domain that interacts with the proteins NIFK and Hklp2 (58, 59). These proteins have been implicated in cancer progression (60) and spindle function (61), respectively, although how these activities may be related to Ki-67 function is not fully clear. Ki-67 also contains a distinct form of a protein phosphatase 1 (PP1)–binding site that is also found in the mitotic exit regulatory protein RepoMan (11); this binding site contributes to efficient removal of mitotic phosphorylation from Ki-67 (15). The majority of Ki-67 is composed of 16 internally repeated ~100–amino acid domains that contain a site for mitotic CDK1 phosphorylation (15, 62). Finally, at the C terminus is an LR domain (63) that binds DNA in vitro (45) and is required for chromosome binding in cells (16, 22). We show that this C-terminal LR domain is necessary and sufficient for

protecting chromosomes from damage during mitosis, either in the presence or absence of p53. This suggests that proteins interacting with Ki-67 domains other than the LR are unlikely to have direct roles in mitotic genome protection. Additionally, these results suggest that the high degree of electrostatic charge across the Ki-67 protein, which is important for maintaining the rod-like shape of individual chromosome arms during mitosis (21, 22), is not required for protection from damage. It remains to be determined whether the Ki-67 C terminus protects chromosomes from damage during mitosis via steric occlusion of enzymes that can inappropriately break DNA strands, or instead physically stabilizes chromosomes in another manner. These are not the only possibilities. For example, the C terminus could be important for recruitment of proteins that protect and/or repair DNA.

What Is the Functional Contribution of p53? p53 is a transcription factor that activates broad responses to DNA damage and other stresses (26, 64). Notably, p53 is mutated in more than half of human cancers (65), and impairing genes that are synthetically lethal with mutated p53 (66) is considered an important path toward therapeutic targets (67). Although most functional contributions of p53 include its activity as a transcription factor, it is clear that the lack of induction of p21 cannot alone account for the Ki-67–p53 synergy, because codepletion of Ki-67 and p21 in hTERT-RPE1 cells results in loss of G1 checkpoint activation but not synthetic lethality (14). Therefore, a transcriptional role for p53 would have to be p21-independent. However, the rapid kinetics of the appearance of damage leads us to favor a more direct role for p53 in sensing and responding to defects caused by Ki-67 depletion.

Which p53 functions may be most relevant to our observations? We note that chromosome missegregation elevates p53 levels, and that p53 limits proliferation of aneuploid cells, contributing to p53's role as a tumor suppressor (68). Therefore, one possibility is that p53's role in monitoring chromosome segregation contributes to our observations. For example, depletion of Ki-67 could result in defective chromosome–kinetochore attachments. In the presence of p53, poor attachments may be recognized and fixed but, in its absence, the observed anaphase bridges may result. Alternatively, DNA strand breaks caused by Ki-67 depletion could be catastrophic in the absence of p53. Kinetochore problems and DNA strand breaks could be interrelated, but whether one or the other is the initiating event remains to be explored.

It is clear that the requirement for Ki-67 to protect cells is much reduced in cells with a CRISPR-engineered p53 deletion (*SI Appendix*, Fig. S6) compared with cells experiencing acute depletion of p53 (Fig. 4). These data suggest that cells adapt to the p53 deletion in a manner that compensates for loss of Ki-67. We hypothesize that this is achieved via altered gene expression and are testing this idea now. We also hypothesize that such adaptation mechanisms could explain apparently contradictory genetic studies in the mouse system, where expression of Ki-67 appears to be nonessential for organismal development (12). Another possibility is that not all of the functions of Ki-67 may be shared between humans and mice.

In conclusion, these studies add to the growing list of important mitotic functions for the human Ki-67 protein. Specifically, we show that the C-terminal chromosome-binding domain of Ki-67 protects human cell DNA from damage during mitotic progression. Ki-67 also is the keystone of the mitotic PCL (11), ensures that mitotic chromosomal arms maintain physical separation (21, 22), and promotes chromosome clustering during mitotic exit, thereby preventing retention of cytoplasmic contents in reforming nuclei (23). It will be of great interest to determine whether these mitotic activities are related to Ki-67's contributions to the organization and silencing of interphase heterochromatin (11–14).

Materials and Methods

Cell Culture. hTERT-RPE1 cells were the same isolate previously studied in the laboratory (14), originally obtained from Judith Sharp and Michael Blower, Boston University School of Medicine, Boston, MA (69). These were cultured in Dulbecco's modified Eagle's medium (DMEM)/F12 media (Gibco; 11320082), 10% fetal bovine serum (FBS) (Avantor Seradigm; VWR), and 100 U/mL penicillin + 100 μg/mL streptomycin. hTERT-RPE1 cells with the p53 gene deleted were a kind gift from Daniel Durocher, Mount Sinai Hospital, Toronto, ON, Canada (56) via Sharon Cantor, University of Massachusetts Medical School (UMMS). HCT116-Ki-67-mAC-AID cells were a kind gift from Masatoshi Takagi, RIKEN, Saitama, Japan (21) and were cultured in DMEM (Gibco; 11995065), 10% FBS, and 100 U/mL penicillin + 100 μg/mL streptomycin. Cells were incubated at 37 °C, 5% CO_2, and 95% humidity.

Antibodies, siRNAs, and PCR primers are listed in Dataset S2.

Cell synchronization. Cells were seeded in 6-well plates containing glass coverslips and grown for 48 h. Cells were first treated according to a double–thymidine block protocol (70) involving two sequential rounds of treatment with 2 mM thymidine in complete culture medium for 18 h, followed by washing with phosphate-buffered saline (PBS) and release into drug-free media for 4 h. Cells were then treated with 10 μM CDK1 inhibitor RO-3306 [Sigma-Aldrich; SML0569 (40, 71)] for 18 h. For some samples, 0.5 mM IAA (Sigma-Aldrich; I5148) was added for the last 6 h of RO-3306 treatment to induce degradation of Ki-67 (21). Some samples were fixed for IF, FACS, or TUNEL analysis prior to release. To release cells from the RO-3306 block, they were washed three times with PBS. "Afterwash" samples were then fixed immediately. Other samples were given fresh drug-free media, and then harvested at the indicated time points.

Assay for Ki-67 transgene function. Cells were seeded in 60-mm culture dishes, grown for 48 h, and then transfected with 1 μg of the indicated plasmids. After 12 h, some cells were treated with 0.5 mM IAA for 24 h, and then at 36 h post transfection all cells were washed with PBS, harvested by trypsinization, and fixed in 70% ethanol in rotating tubes for 20 min. Cells were blocked for 1 h at 4 °C using 1% bovine serum albumin (BSA) in PBS + 0.1% Triton X-100, and then primary antibodies (1 mL diluted 1:1,000 in blocking buffer) were added for incubation overnight in 1.5-mL microfuge tubes on a rotator at 4 °C. Cells were then washed three times with PBS + 0.1% Triton X-100, collecting cells by centrifugation for 1 min at 2,000 × *g* and removing the supernatant by aspiration. Secondary fluorescent antibodies (1:2,000 in blocking buffer) were incubated for 1 h in a tube rotator at room temperature. Cells were washed three times with PBS + 0.1% Triton X-100, labeled with 1 μM DAPI diluted in PBS, and washed twice with PBS + 1% BSA + 0.1% Triton X-100 prior to analysis by flow cytometry.

Flow cytometry. Labeled cells were filtered through 37-μm nylon mesh to enrich for single cells and analyzed in the UMMS flow cytometry core on a BD LSR II flow cytometer, using wavelengths of 405 nm for DAPI, 488 nm for mClover-tagged Ki-67, and 647 nm for Alexa Fluor 647–labeled secondary antibodies (for γH2AX). Ten thousand cells were analyzed for each sample. Samples were analyzed using BD LSR II and BD Celesta instruments. Data files (.fcs) were analyzed using FlowJo v10.6.2 or FCS Express 7.06.0015 and plotted with linear axes.

Amnis FACS was performed using a FlowSight image cytometer (Luminex) with a 20× at 0.6 numerical aperture objective with 1-μm pixel size. Images were analyzed using Ideas 6.0 software.

Transfection. Plasmids encoding GFP-tagged Ki-67 transgenes were a kind gift from Masatoshi Takagi (16). To make the pPK1020 plasmid in which the EF1α promoter drives expression of human p53, the 2.5-kb NheI–NotI fragment from pIRES-GFP-p53wt [Addgene; 49242 (72)] was inserted into SpeI + NotI–digested pEF-ENTR-A (73).

DNA was purified for transfection using ZymoPURE Midiprep Kits (Zymo Research). Plasmid transfections were accomplished using Lipofectamine 2000 (Invitrogen). Twelve hours after plasmid transfections, HCT116 cells were either untreated or treated for 24 h with 0.5 mM IAA, and then analyzed by flow cytometry or immunofluorescence.

siRNA transfections were performed using Lipofectamine RNAiMAX (Invitrogen) as recommended by the manufacturer. siRNA duplexes were purchased from Ambion (Life Technologies). si-Ki-67 was used at a concentration of 20 μM, si-p21 was used at 40 μM, and siRNAs targeting p53 were used at 80 μM. Concentrations of the silencing control siRNA ("scr") were matched with the experimental duplex for each experiment. hTERT-RPE1 and HCT116 cells were analyzed 72 h after siRNA transfections, with phleomycin treatments for the last 5 h where indicated.

Immunofluorescence studies. Cells were seeded in tissue culture–treated 6-well plates for 48 h, and then transfected with siRNAs. In some HCT116 experiments, cells were treated with 500 μM IAA for 24 h prior to harvest to deplete Ki-67. Seventy-two hours after transfection, cells were washed twice

with PBS and fixed in 4% paraformaldehyde diluted in PBS for 10 min at room temperature. Cells were then washed twice with PBS, treated with ice-cold methanol for 20 min at −20 °C, and blocked for 1 h at 4 °C in PBS + 1% BSA + 0.1% Triton X-100. Antibodies were diluted in the same blocking buffer, and added to fixed cells overnight at 4 °C. Cells were then washed three times, 5 min each, with PBS. Secondary fluorescent antibodies were diluted 1:1,000 in the same blocking buffer and then added to cells and incubated for 1 h at room temperature in a dark container. Cells were washed three times with PBS for 5 min each, and then counterstained with 1 μM DAPI for 1 min. Cells were washed twice with PBS, and the coverslips were mounted on glass slides using ProLong Gold Antifade (Invitrogen; P36934). Nuclei were marked as regions of interest and average signal intensities were measured using Zeiss Zen blue software for each analyzed nucleus. IF intensity measurement statistics were analyzed using GraphPad Prism.

Visualization of EdU-labeled nascent DNA. HCT116 cells were grown on glass coverslips in DMEM as described above. EdU (Sigma; T511285-5MG) was added to the culture medium at 10 μM for 30 min. After labeling, cells were washed three times with PBS. Cells were fixed in 4% formaldehyde for 20 min. Cells were then rinsed twice with PBS + 0.1% Triton X-100 and then incubated for 30 min in 100 mM Tris·HCl (pH 8.5), 1 mM $CuSO_4$, 100 mM ascorbic acid, and 50 mM MB-Fluor 595 azide (Click Chemistry Tools; 1169-5) for click-chemistry labeling (14, 74). After staining, the cells on coverslips were washed three times with PBS + 0.5% Triton X-100 for 5 min each. Cells were then counterstained with DAPI, mounted onto microscope slides, and imaged by fluorescence microscopy as described above.

Imaging. Images were acquired using a Zeiss LSM 700 confocal microscope equipped with laser lines of 405/488/594/647 nm and suitable emission filters. A Plan-Apochromat 63×/1.40 oil differential interference contrast m27 objective was used. For analysis of 53BP1 foci, a Zeiss Axio Observer epifluorescence microscope with mounted Axiocam 506 monochrome camera and automated stage was used. Data were analyzed using Zeiss Zen blue software.

Additional methods for RNA isolation, qPCR, RNA-seq, TUNEL assays, cell-proliferation assays, tests of zVAD-FMK, and plasmid complementation assays are described in *SI Appendix*.

Data Availability. The RNA-seq data reported in this article have been deposited in the Gene Expression Omnibus (accession no. GSE159160) (75). All study data are included in the main text and supporting information.

ACKNOWLEDGMENTS. We thank Judith Sharp and Sharon Cantor for helpful comments on the manuscript. These studies were funded by Grant R35 GM127035 from the NIH (to P.D.K.). We thank Judith Sharp and Michael Blower for the hTERT-RPE1 cells, Daniel Durocher and Sharon Cantor for the hTERT-RPE1 $p53^{-/-}$ cells, and Masatoshi Takagi for the generous gift of plasmids and the HCT116-Ki-67-mAC cells.

1. X. Sun, P. D. Kaufman, Ki-67: More than a proliferation marker. *Chromosoma* **127**, 175–186 (2018).
2. M. Sobecki *et al.*, Cell-cycle regulation accounts for variability in Ki-67 expression levels. *Cancer Res.* **77**, 2722–2734 (2017).
3. I. Miller *et al.*, Ki67 is a graded rather than a binary marker of proliferation versus quiescence. *Cell Rep.* **24**, 1105–1112.e5 (2018).
4. J.-S. Pyo, G. Kang, J. H. Sohn, Ki-67 labeling index can be used as a prognostic marker in gastrointestinal stromal tumor: A systematic review and meta-analysis. *Int. J. Biol. Markers* **31**, e204–e210 (2016).
5. R. Pezzilli *et al.*, Ki-67 prognostic and therapeutic decision driven marker for pancreatic neuroendocrine neoplasms (PNENs): A systematic review. *Adv. Med. Sci.* **61**, 147–153 (2016).
6. S. Richards-Taylor *et al.*, The assessment of Ki-67 as a prognostic marker in neuroendocrine tumours: A systematic review and meta-analysis. *J. Clin. Pathol.* **69**, 612–618 (2016).
7. W. Wang *et al.*, A Ki-67 index to predict treatment response to the capecitabine temozolomide (CAPTEM) regimen in neuroendocrine neoplasms: A retrospective multicenter study. *Neuroendocrinology*, 10.1159/000510159 (2020).
8. K. Mrouj *et al.*, Ki-67 regulates global gene expression and promotes sequential stages of carcinogenesis. *Proc. Natl. Acad. Sci. U.S.A.* **118**, e2026507118 (2021).
9. J. Gerdes *et al.*, Cell cycle analysis of a cell proliferation-associated human nuclear antigen defined by the monoclonal antibody Ki-67. *J. Immunol.* **133**, 1710–1715 (1984).
10. I. R. Kill, Localisation of the Ki-67 antigen within the nucleolus. Evidence for a fibrillarin-deficient region of the dense fibrillar component. *J. Cell Sci.* **109**, 1253–1263 (1996).
11. D. G. Booth *et al.*, Ki-67 is a PP1-interacting protein that organises the mitotic chromosome periphery. *eLife* **3**, e01641 (2014).
12. M. Sobecki *et al.*, The cell proliferation antigen Ki-67 organises heterochromatin. *eLife* **5**, e13722 (2016).
13. T. D. Matheson, P. D. Kaufman, The p150N domain of chromatin assembly factor-1 regulates Ki-67 accumulation on the mitotic perichromosomal layer. *Mol. Biol. Cell* **28**, 21–29 (2017).
14. X. Sun *et al.*, Ki-67 contributes to normal cell cycle progression and inactive X heterochromatin in p21 checkpoint-proficient human cells. *Mol. Cell. Biol.* **37**, e00569-16 (2017).
15. M. Takagi, Y. Nishiyama, A. Taguchi, N. Imamoto, Ki67 antigen contributes to the timely accumulation of protein phosphatase 1γ on anaphase chromosomes. *J. Biol. Chem.* **289**, 22877–22887 (2014).
16. T. Saiwaki, I. Kotera, M. Sasaki, M. Takagi, Y. Yoneda, In vivo dynamics and kinetics of pKi-67: Transition from a mobile to an immobile form at the onset of anaphase. *Exp. Cell Res.* **308**, 123–134 (2005).
17. D. G. Booth *et al.*, 3D-CLEM reveals that a major portion of mitotic chromosomes is not chromatin. *Mol. Cell* **64**, 790–802 (2016).
18. T. D. Matheson, P. D. Kaufman, Grabbing the genome by the NADs. *Chromosoma* **125**, 361–371 (2016).
19. D. G. Booth, W. C. Earnshaw, Ki-67 and the chromosome periphery compartment in mitosis. *Trends Cell Biol.* **27**, 906–916 (2017).
20. A. A. Van Hooser, P. Yuh, R. Heald, The perichromosomal layer. *Chromosoma* **114**, 377–388 (2005).
21. M. Takagi, T. Natsume, M. T. Kanemaki, N. Imamoto, Perichromosomal protein Ki67 supports mitotic chromosome architecture. *Genes Cells* **21**, 1113–1124 (2016).
22. S. Cuylen *et al.*, Ki-67 acts as a biological surfactant to disperse mitotic chromosomes. *Nature* **535**, 308–312 (2016).
23. S. Cuylen-Haering *et al.*, Chromosome clustering by Ki-67 excludes cytoplasm during nuclear assembly. *Nature* **587**, 285–290 (2020).
24. M. Takagi *et al.*, Ki-67 and condensins support the integrity of mitotic chromosomes through distinct mechanisms. *J. Cell Sci.* **131**, jcs212092 (2018).
25. W. S. el-Deiry *et al.*, WAF1, a potential mediator of p53 tumor suppression. *Cell* **75**, 817–825 (1993).
26. M. Fischer, P. Grossmann, M. Padi, J. A. DeCaprio, Integration of TP53, DREAM, MMB-FOXM1 and RB-E2F target gene analyses identifies cell cycle gene regulatory networks. *Nucleic Acids Res.* **44**, 6070–6086 (2016).
27. E. M. Hatch, A. H. Fischer, T. J. Deerinck, M. W. Hetzer, Catastrophic nuclear envelope collapse in cancer cell micronuclei. *Cell* **154**, 47–60 (2013).
28. S. Liu *et al.*, Nuclear envelope assembly defects link mitotic errors to chromothripsis. *Nature* **561**, 551–555 (2018).
29. E. P. Rogakou, D. R. Pilch, A. H. Orr, V. S. Ivanova, W. M. Bonner, DNA double-stranded breaks induce histone H2AX phosphorylation on serine 139. *J. Biol. Chem.* **273**, 5858–5868 (1998).
30. J. F. Koy *et al.*, Genetic changes and bioassays in bleomycin- and phleomycin-treated cells, and their relationship to chromosomal breaks. *Mutat. Res.* **336**, 19–27 (1995).
31. L. B. Schultz, N. H. Chehab, A. Malikzay, T. D. Halazonetis, p53 binding protein 1 (53BP1) is an early participant in the cellular response to DNA double-strand breaks. *J. Cell Biol.* **151**, 1381–1390 (2000).
32. I. Rappold, K. Iwabuchi, T. Date, J. Chen, Tumor suppressor p53 binding protein 1 (53BP1) is involved in DNA damage-signaling pathways. *J. Cell Biol.* **153**, 613–620 (2001).
33. B. Wang, S. Matsuoka, P. B. Carpenter, S. J. Elledge, 53BP1, a mediator of the DNA damage checkpoint. *Science* **298**, 1435–1438 (2002).
34. M. Zimmermann, T. de Lange, 53BP1: Pro choice in DNA repair. *Trends Cell Biol.* **24**, 108–117 (2014).
35. R. E. Kleiner, P. Verma, K. R. Molloy, B. T. Chait, T. M. Kapoor, Chemical proteomics reveals a γH2AX-53BP1 interaction in the DNA damage response. *Nat. Chem. Biol.* **11**, 807–814 (2015).
36. C. Lukas *et al.*, 53BP1 nuclear bodies form around DNA lesions generated by mitotic transmission of chromosomes under replication stress. *Nat. Cell Biol.* **13**, 243–253 (2011).
37. G. Nelson, M. Buhmann, T. von Zglinicki, DNA damage foci in mitosis are devoid of 53BP1. *Cell Cycle* **8**, 3379–3383 (2009).
38. Y. Gavrieli, Y. Sherman, S. A. Ben-Sasson, Identification of programmed cell death in situ via specific labeling of nuclear DNA fragmentation. *J. Cell Biol.* **119**, 493–501 (1992).
39. D. R. Whelan *et al.*, Super-resolution visualization of distinct stalled and broken replication fork structures. *PLoS Genet.* **16**, e1009256 (2020).
40. L. T. Vassilev *et al.*, Selective small-molecule inhibitor reveals critical mitotic functions of human CDK1. *Proc. Natl. Acad. Sci. U.S.A.* **103**, 10660–10665 (2006).
41. B. D. Larsen, C. S. Sørensen, The caspase-activated DNase: Apoptosis and beyond. *FEBS J.* **284**, 1160–1170 (2017).
42. E. A. Slee *et al.*, Benzyloxycarbonyl-Val-Ala-Asp (OMe) fluoromethylketone (Z-VAD.FMK) inhibits apoptosis by blocking the processing of CPP32. *Biochem. J.* **315**, 21–24 (1996).
43. P. Pantazis, J. A. Early, J. T. Mendoza, A. R. DeJesus, B. C. Giovanella, Cytotoxic efficacy of 9-nitrocamptothecin in the treatment of human malignant melanoma cells in vitro. *Cancer Res.* **54**, 771–776 (1994).
44. Z. Han *et al.*, Role of p21 in apoptosis and senescence of human colon cancer cells treated with camptothecin. *J. Biol. Chem.* **277**, 17154–17160 (2002).
45. D. E. MacCallum, P. A. Hall, The biochemical characterization of the DNA binding activity of pKi67. *J. Pathol.* **191**, 286–298 (2000).
46. M. Fenech *et al.*, Molecular mechanisms of micronucleus, nucleoplasmic bridge and nuclear bud formation in mammalian and human cells. *Mutagenesis* **26**, 125–132 (2011).

47. U. Ben-David, A. Amon, Context is everything: Aneuploidy in cancer. *Nat. Rev. Genet.* **21**, 44–62 (2020).
48. M. Vietri *et al*., Unrestrained ESCRT-III drives micronuclear catastrophe and chromosome fragmentation. *Nat. Cell Biol.* **22**, 856–867 (2020).
49. D. R. Hoffelder *et al*., Resolution of anaphase bridges in cancer cells. *Chromosoma* **112**, 389–397 (2004).
50. X. Guo *et al*., Understanding the birth of rupture-prone and irreparable micronuclei. *Chromosoma* **129**, 181–200 (2020).
51. N. T. Umbreit *et al*., Mechanisms generating cancer genome complexity from a single cell division error. *Science* **368**, eaba0712 (2020).
52. I. E. Wassing *et al*., The RAD51 recombinase protects mitotic chromatin in human cells. *bioRxiv* [Preprint] (2020). https://doi.org/10.1101/2020.08.11.246231 (accessed 11 August 2020).
53. K. L. McKinley, I. M. Cheeseman, Large-scale analysis of CRISPR/Cas9 cell-cycle knockouts reveals the diversity of p53-dependent responses to cell-cycle defects. *Dev. Cell* **40**, 405–420.e2 (2017).
54. M. Olivieri *et al*., A genetic map of the response to DNA damage in human cells. *Cell* **182**, 481–496.e21 (2020).
55. A. R. Bowden *et al*., Parallel CRISPR-Cas9 screens clarify impacts of p53 on screen performance. *eLife* **9**, e55325 (2020).
56. M. Zimmermann *et al*., CRISPR screens identify genomic ribonucleotides as a source of PARP-trapping lesions. *Nature* **559**, 285–289 (2018).
57. L. Bury *et al*., Alpha-satellite RNA transcripts are repressed by centromere-nucleolus associations. *eLife* **9**, e59770 (2020).
58. M. Sueishi, M. Takagi, Y. Yoneda, The forkhead-associated domain of Ki-67 antigen interacts with the novel kinesin-like protein Hklp2. *J. Biol. Chem.* **275**, 28888–28892 (2000).
59. M. Takagi, M. Sueishi, T. Saiwaki, A. Kametaka, Y. Yoneda, A novel nucleolar protein, NIFK, interacts with the forkhead associated domain of Ki-67 antigen in mitosis. *J. Biol. Chem.* **276**, 25386–25391 (2001).
60. T.-C. Lin *et al*., The nucleolar protein NIFK promotes cancer progression via CK1α/β-catenin in metastasis and Ki-67-dependent cell proliferation. *eLife* **5**, e11288 (2016).
61. D. Vanneste, M. Takagi, N. Imamoto, I. Vernos, The role of Hklp2 in the stabilization and maintenance of spindle bipolarity. *Curr. Biol.* **19**, 1712–1717 (2009).
62. C. Schlüter *et al*., The cell proliferation-associated antigen of antibody Ki-67: A very large, ubiquitous nuclear protein with numerous repeated elements, representing a new kind of cell cycle-maintaining proteins. *J. Cell Biol.* **123**, 513–522 (1993).
63. M. Takagi, Y. Matsuoka, T. Kurihara, Y. Yoneda, Chmadrin: A novel Ki-67 antigen-related perichromosomal protein possibly implicated in higher order chromatin structure. *J. Cell Sci.* **112**, 2463–2472 (1999).
64. J. Campisi, Suppressing cancer: The importance of being senescent. *Science* **309**, 886–887 (2005).
65. S. Morandell, M. B. Yaffe, Exploiting synthetic lethal interactions between DNA damage signaling, checkpoint control, and p53 for targeted cancer therapy. *Prog. Mol. Biol. Transl. Sci.* **110**, 289–314 (2012).
66. X. Wang, R. Simon, Identification of potential synthetic lethal genes to p53 using a computational biology approach. *BMC Med. Genomics* **6**, 30 (2013).
67. H. C. Reinhardt, H. Jiang, M. T. Hemann, M. B. Yaffe, Exploiting synthetic lethal interactions for targeted cancer therapy. *Cell Cycle* **8**, 3112–3119 (2009).
68. S. L. Thompson, D. A. Compton, Proliferation of aneuploid human cells is limited by a p53-dependent mechanism. *J. Cell Biol.* **188**, 369–381 (2010).
69. J. A. Sharp, C. Perea-Resa, W. Wang, M. D. Blower, Cell division requires RNA eviction from condensing chromosomes. *J. Cell Biol.* **219**, e201910148 (2020).
70. G. Chen, X. Deng, Cell synchronization by double thymidine block. *Bio Protoc.* **8**, e2994 (2018).
71. H. T. Ma, R. Y. C. Poon, Synchronization of HeLa cells. *Methods Mol. Biol.* **1524**, 189–201 (2017).
72. S. C. Lin, E. D. Karoly, D. J. Taatjes, The human ΔNp53 isoform triggers metabolic and gene expression changes that activate mTOR and alter mitochondrial function. *Aging Cell* **12**, 863–872 (2013).
73. E. Campeau *et al*., A versatile viral system for expression and depletion of proteins in mammalian cells. *PLoS One* **4**, e6529 (2009).
74. C. L. Smith *et al*., A separable domain of the p150 subunit of human chromatin assembly factor-1 promotes protein and chromosome associations with nucleoli. *Mol. Biol. Cell* **25**, 2866–2881 (2014).
75. O. Garwain, R. Li, L. J. Zhu, P. D. Kaufman, Raw RNA-seq data from control and Ki-67-depleted HCT116 human colon cancer cells. *Gene Expression Omnibus*. https://www.ncbi.nlm.nih.gov/geo/query/acc.cgi?acc=GSE1591605. Deposited 7 October 2020.